



Influence of winter Arctic sea ice concentration change on the El Niño–Southern Oscillation in the following winter

Shangfeng Chen^{1,4} · Renguang Wu² · Wen Chen^{1,4} · Bin Yu³

Received: 10 May 2019 / Accepted: 23 October 2019 / Published online: 5 November 2019
© Springer-Verlag GmbH Germany, part of Springer Nature 2019

Abstract

The present study reveals a close connection between the winter Arctic sea ice concentration (ASIC) change over the Greenland–Barents Seas (GBS) and the El Niño–Southern Oscillation (ENSO) in the following winter. When there is more winter ASIC over the GBS, an El Niño-like sea surface temperature (SST) warming tends to occur in the tropical central-eastern Pacific (TCEP) during the following winter. It is found that the winter ASIC increase over the GBS triggers an atmospheric wave train propagating southeastward from the high latitude Eurasia towards the subtropical North Pacific, with cyclonic wind anomalies over the subtropical North Pacific. A barotropic model experiment with anomalous convergence prescribed around the GBS reproduces reasonably well the atmospheric wave train. The induced spring SST warming and associated anomalous atmospheric heating over the subtropical North Pacific play an essential role in the formation and maintenance of lower-level westerly wind anomalies over the western tropical Pacific. These westerly wind anomalies induce SST warming in the TCEP during the following summer via triggering an eastward propagating equatorial warm Kelvin wave. The summer TCEP SST warming further develops into an El Niño event in the following winter via a Bjerknes-like positive air–sea feedback process. This result suggests that the winter ASIC change around the GBS is a potential predictor of the ENSO events with a lead time of 1 year.

Keywords Arctic sea ice · ENSO · Atmospheric wave train · Westerly winds

1 Introduction

El Niño–Southern Oscillation (ENSO) is the strongest air–sea coupled mode over the tropical Pacific on the inter-annual timescale (e.g., Philander 1985; Lau and Nath 1996; Zhang et al. 1997; Wang et al. 2000; Alexander et al. 2002;

Yu and Zwiers 2007). A number of studies have demonstrated that the ENSO events (El Niño and La Niña) can exert considerable influences on the agriculture, corals, fire risks, and extreme weather and climate events over many regions of the world (Glynn and de Weerd 1991; Bell et al. 1999; Chen et al. 2000; Chan and Zhou 2005; McPhaden et al. 2006; Burn and Whitfield 2015; Barbero et al. 2015; Song et al. 2017; Ding et al. 2018; He et al. 2018; Hu et al. 2018; Chen and Song 2019; and references therein). For example, the extreme high temperature and dry conditions over the Amazon Basin from mid-2009 to mid-2010 were due largely to the El Niño event in the Pacific (Ropelewski and Halpert 1987; Lewis et al. 2011). The strong 2010–2011 La Niña event contributed notably to the occurrence of severe high temperature and drought (low temperature and wet) events over south (north) America (Burn and Whitfield 2015). In addition, ENSO events can exert substantial impacts on the East Asian monsoon and related surface temperature and precipitation anomalies over East Asia primarily via inducing an anomalous anticyclone/cyclone over the western North Pacific (WNP) (Wang et al. 2000; Wu

Electronic supplementary material The online version of this article (<https://doi.org/10.1007/s00382-019-05027-1>) contains supplementary material, which is available to authorized users.

✉ Shangfeng Chen
chenshangfeng@mail.iap.ac.cn

- ¹ Center for Monsoon System Research, Institute of Atmospheric Physics, Chinese Academy of Sciences, Beijing, China
- ² School of Earth Sciences, Zhejiang University, Hangzhou, China
- ³ Climate Research Division, Environment and Climate Change Canada, Toronto, ON, Canada
- ⁴ University of Chinese Academy of Sciences, Beijing, China

et al. 2003) as well as on the European climate variation via atmospheric teleconnections (Graf and Zanchettin 2012). Furthermore, tropical cyclone activities (one of the worst natural disasters in the world) over the WNP and Atlantic were also significantly modulated by ENSO events (Gray 1984; Chan 2005).

Due to the impact of ENSO on global climate, understanding the factors of ENSO occurrence and the underlying mechanisms is of great importance. Studies have demonstrated the important roles of the processes within the tropical Pacific, including the positive air–sea feedback and oceanic dynamics in the ENSO occurrence (Bjerknes 1969; Schopf and Suarez 1988; Jin 1997; Latif et al. 1998). In addition, studies have suggested that the atmosphere–ocean variability over the extratropics plays a non-negligible role in modulating sea surface temperature (SST) anomalies in the tropical central-eastern Pacific (TCEP) related to ENSO (Li 1990; Vimont et al. 2001, 2003; Nakamura et al. 2006, 2007; Wang et al. 2011; Park et al. 2013; Chen et al. 2014a, 2016a, 2018a, b, c). Li (1990) found that an enhanced cold surge activity induced by stronger East Asian winter monsoon tends to enhance atmospheric heating anomalies over the WNP. The anomalous atmospheric heating brings the westerly wind burst over the western tropical Pacific (WTP), which is followed by the outbreak of an El Niño event in the following winter via triggering an eastward propagating equatorial warm Kelvin wave. Vimont et al. (2001) demonstrated that the boreal wintertime North Pacific Oscillation-related atmospheric circulation anomaly (Walker and Bliss 1932; Rogers 1981) is an important trigger for the outbreak of an ENSO event via the so-called seasonal footprinting mechanism. Nakamura et al. (2006) reported that the spring Arctic Oscillation (AO, Thompson and Wallace 1998; He 2015) influences the occurrence of El Niño events in the following winter via modulating the westerly wind anomalies over the WTP. In addition, recent studies suggested notable impacts of SST anomalies in the mid-latitudes of the North Pacific and the North Atlantic on the ENSO occurrence via modulating the westerly wind anomalies over the WTP (Wang et al. 2011; Ham et al. 2013; Chen et al. 2018c). Previous studies have demonstrated that the winter–spring westerly wind anomalies over the WTP are an important trigger for the outbreak of an El Niño event in the following winter via triggering eastward propagating warm Kelvin waves (Li 1990; Vimont et al. 2003, Nakamura et al. 2006, 2007; Chen et al. 2014a).

Arctic sea ice is one of the most important components of the Earth's climate system. Arctic sea ice changes exert large influences on weather and climate over the mid-high latitudes of the Northern Hemisphere (NH) (Francis et al. 2009; Honda et al. 2009; Wu et al. 2011, 2016; Liu et al. 2012; Cohen et al. 2012; Li and Wu 2012; Li and Wang 2013; Screen et al. 2014; Chen et al. 2014b; Kug et al. 2015;

Xu et al. 2018; Chen and Wu 2018; He et al. 2018; Chen et al. 2019a, b; Li et al. 2019). For example, the Arctic sea ice change is found to impact the East Asian winter monsoon activity via modulating the blocking high over the Eurasian continent (Wu et al. 2011). Recent extreme cold winters over the NH midlatitudes tend to be related to the Arctic sea ice loss (Liu et al. 2012). Decrease in the Arctic Sea ice concentration (ASIC) over the Norwegian–Barents Sea during boreal winter induces above-normal rainfall over East Asia during the subsequent spring by triggering an atmospheric wave train over the Eurasian continent (Wu et al. 2016). It should be noted that although statistically significant linkages between the Arctic sea ice change and mid-latitude climate variations have been identified by many previous studies, the underlying physical processes for the connections are still a controversial topic and remain to be explored (Gao et al. 2015).

The possible connection between the ENSO variability and the Arctic sea ice change has been investigated in previous studies. Jevrejeva et al. (2003) indicated that the Arctic sea ice variability over the Baltic Sea has a close relationship with the SST anomalies in the Niño-3 region (5°S–5°N and 90°–150°W) on the 12–20 year periodicity. Liu et al. (2004) found that El Niño events can lead to decrease (increase) in the Arctic Sea ice over the Chukchi–Beaufort Seas (the Northwest Passage) via modulating the mean meridional heat flux induced by the regional Ferrel cell change. Hu et al. (2016) suggested that the central Pacific El Niño-related SST anomalies tend to slow down the summer Arctic warming and sea-ice melting through increasing the circumpolar westerly winds.

The above studies focused on investigation of either the influence of ENSO on the ASIC or the impacts of ENSO and ASIC changes on weather and climate. It remains unclear whether changes in the ASIC can influence the subsequent winter ENSO occurrence, which has important implications for the ENSO prediction. Our analysis found that the inter-annual variation of the ASIC around the Greenland–Barents Seas (GBS) in preceding winter can exert a significant influence on the outbreak of ENSO events in the following winter via modulating the westerly wind anomalies over the WTP. The finding highlights the remote influence of the preceding ASIC change on the succeeding tropical Pacific atmosphere–ocean system. The present study investigates the connection between ASIC and ENSO and the associated physical processes.

The remainder of this paper is organized as follows. Section 2 describes the data and methods. Section 3 presents observational evidence to demonstrate the relationship between the preceding ASIC change and the following winter ENSO. Section 4 discusses the physical process responsible for the ASIC influence on ENSO. Section 5 provides a summary and discussion.

2 Data and methods

2.1 Data

The present study uses monthly mean sea level pressure (SLP), geopotential heights and winds in the troposphere, precipitation, surface zonal wind stress, and surface heat fluxes (including surface latent and sensible heat fluxes, and surface longwave and shortwave radiations) from the National Centers for Environmental Prediction–National Center for Atmospheric Research (NCEP–NCAR) reanalysis (Kalnay et al. 1996; <http://www.esrl.noaa.gov/psd/data/gridded/data.ncep.reanalysis.derived.html>), which are available from 1948 to the present. SLP, winds, geopotential height, omega have a horizontal resolution of $2.5^\circ \times 2.5^\circ$ in latitude–longitude grids. Surface heat fluxes, precipitation, and zonal wind stress are in T62 horizontal Gaussian grids. This study also employs the monthly ASIC data provided by the Met Office Hadley Centre Sea Ice and Sea Surface Temperature (HadISST) dataset version 1.1 (Rayner et al. 2003; <https://www.metoffice.gov.uk/hadobs/hadisst/>), which is available from 1870 to the present and has a horizontal resolution of $1^\circ \times 1^\circ$.

This analysis employs three monthly mean SST datasets. They are the National Oceanic and Atmospheric Administration (NOAA) Extended Reconstructed SST version 3b (ERSSTv3b, Smith et al. 2008; <https://www.esrl.noaa.gov/psd/data/gridded/data.noaa.ersst.html>), the NOAA Extended Reconstructed SST version 5 (ERSSTv5, Huang et al. 2017; <https://www.esrl.noaa.gov/psd/data/gridded/data.noaa.ersst.v5.html>), and the HadISST version 1.1 (Rayner et al. 2003; <https://www.metoffice.gov.uk/hadobs/hadisst/>). Both ERSSTv3b and ERSSTv5 SST datasets have a horizontal resolution of $2^\circ \times 2^\circ$ and cover the period from 1854 to the present. The HadISST dataset is available since 1870 and has a horizontal resolution of $1^\circ \times 1^\circ$.

This study focuses on the variation on the interannual timescale. Therefore, anomalies of all the variables are subjected to a 7-year high pass Lanczos filter (Duchon 1979) to obtain their interannual components. Using a 5-year, 9-year or 11-year high pass filter leads to similar results (not shown). Significance levels of the correlation and regression coefficients and the composite anomalies are estimated according to a two-tailed Student’s *t* test. ENSO variability is characterized by the Niño-3.4 index, which is defined as area-mean SST anomalies over the region of $5^\circ\text{S}–5^\circ\text{N}$ and $120^\circ–170^\circ\text{W}$. An ASIC index is defined as the area-averaged winter ASIC anomalies over the region of $70^\circ–80^\circ\text{N}$, $10^\circ\text{W}–50^\circ\text{E}$ where significant ASIC anomalies associated with the preceding winter Niño-3.4 index are detected (Fig. 1), as will be described

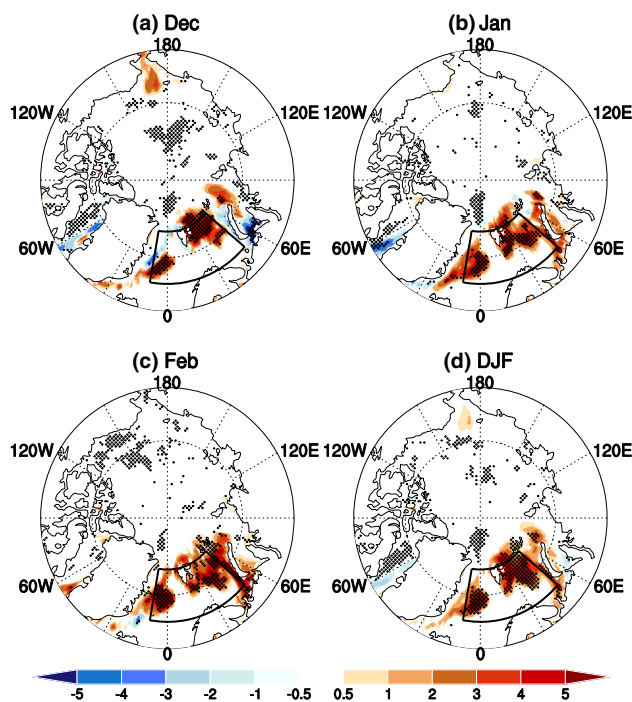


Fig. 1 Arctic sea ice concentration (ASIC) anomalies (unit: %) at preceding **a** December (Dec(− 1)), **b** January (Jan(0)), **c** February (Feb(0)), and **d** December–January–February-mean (D(− 1)JF(0)) obtained by regression upon the standardized Niño-3.4 index during following winter (D(0)JF(1)) over period 1980–2019. Stippling regions indicate ASIC anomalies that are significantly different from zero at the 95% confidence level according to the two-tailed Student’s *t* test. The black boxes in **a–d** represent the region ($70^\circ–80^\circ\text{N}$, $10^\circ\text{W}–50^\circ\text{E}$) that is used to define the ASIC index. Niño-3.4 index is calculated based on the ERSSTv3b SST dataset

below. Note that the ASIC anomalies have been weighted by the cosine of the latitude to account for decrease of area towards north before calculating the ASIC index. Arctic sea ice concentration data provided by the HadISSTv1.1 is relatively unreliable prior to 1979 (the start of satellite era). Hence, the analysis in this study is constrained to the period after 1979.

2.2 Wave activity flux

The wave activity flux proposed by Takaya and Nakamura (1997, 2001) is employed to examine the stationary Rossby wave propagation. This wave activity flux is parallel to the local group velocity of the stationary wave train in a Wentzel–Kramers–Brillouin approximation, and is unrelated to the wave phase. The wave activity flux can be written as follows:

$$W = \frac{1}{2|U|} \begin{pmatrix} U(v'^2 - \psi'v'_x) + V(-u'v' + \psi'u'_x) \\ U(-u'v' + \psi'u'_x) + V(u'^2 + \psi'u'_y) \\ \frac{f_0 R_{ad}}{N^2 H_0} \{ U(v'T' - \psi'T'_x) + V(-u'T' - \psi'T'_y) \} \end{pmatrix}$$

where ψ' is perturbed geostrophic stream function, $V = (u', v')$ and $U = (U, V)$ stand for perturbed geostrophic winds and mean winds, respectively. H_o is the scale height, T' is perturbed air temperature, p is pressure standardized by 1000 hPa. R_a , f_o , and N represent gas constant related to the dry air, the Coriolis parameter at 45°N and the Brunt–Vaisala frequency, respectively. The subscripts x and y indicate derivatives in the zonal and meridional directions, respectively.

2.3 Rossby wave sources

The linearized Rossby wave source (Sardeshmukh and Hoskins 1988) is expressed as follows:

$$S = -\overline{v'_x} \nabla \zeta' - \zeta' \nabla \cdot \overline{v'_x} - \overline{v'_x} \nabla \zeta - \zeta \nabla \cdot \overline{v'_x},$$

where $\overline{v'_x}$ represents horizontal components of the divergent wind, and ζ denotes absolute vorticity. In this study, overbar represents the long-term climatological mean and prime denotes composite anomalies between positive and negative ASIC winters.

2.4 Kelvin wave forcing function

The equatorially oceanic Kelvin wave forcing function (Battisti 1988; Vimont et al. 2003) is used to describe the dynamic response of tropical ocean to surface zonal wind stress anomaly, which is expressed as follows:

$$K_f(x, \lambda) = \int_{30S}^{30N} \tau_x(x, y, \lambda) \psi_0(y) dy,$$

where x and y represent the longitude and latitude, respectively. $\tau_x(x, y, \lambda)$ denotes anomalous surface zonal wind stress at a given lag time λ . $\psi_0(y)$ is the meridional equatorial Kelvin wave structure. Positive (negative) value of K_f corresponds to surface zonal wind anomalies that trigger an eastward propagating and downwelling (upwelling) equatorial Kelvin wave, which contributes to SST warming (cooling).

2.5 Linear barotropic model

This study uses a barotropic model to verify contribution of ASIC change to the generation of a quasi-barotropic atmospheric wave train over Eurasia. As suggested by previous studies (Sardeshmukh and Hoskins 1988; Watanabe 2004; Chen et al. 2016b), the linear barotropic model can well capture atmospheric anomalies triggered by anomalous divergence/convergence over the upper troposphere. The barotropic model consists of a simple barotropic vorticity equation as follows (Sardeshmukh and Hoskins 1988):

$$J(\overline{\psi}, \nabla^2 \psi') + J(\psi', \nabla^2 \overline{\psi} + f) + \gamma \nabla^6 \psi' + \delta \nabla^2 \psi' = S'$$

Here J and $\overline{\psi}$ are the Jacobin operator and mean streamfunction, respectively. ψ' represents the perturbation of the streamfunction. f is the Coriolis parameter. S' is the vorticity source attributed to divergence/convergence anomalies over upper troposphere. δ and γ are the Rayleigh friction and biharmonic diffusion coefficients, respectively.

3 Relation between the winter ASIC and the following winter ENSO

In this section, we present evidence for the connection between ASIC and ENSO. We first show signals of ENSO in the Arctic sea ice. Then, we examine their temporal relationship. Afterward, we document tropical Pacific SST and atmospheric circulation anomalies associated with ASIC.

Obvious Arctic sea ice signal is detected in preceding winter of ENSO events. Figure 1 shows regressions of ASIC anomalies in December(−1), January(0), February(0), and December(−1)–January(0)–February(0) (D(−1)JF(0)) mean upon the following winter Niño-3.4 index during 1980–2019. Niño-3.4 index is calculated based on the ERSSTv3b SST dataset. Here, notations of “(−1)”, “(0)”, and “(1)” denote the years before, during, and after the ENSO developing phase, respectively. Spatial distributions of the ASIC anomalies are similar in Dec(−1), Jan(0), and Feb(0), with significant positive ASIC anomalies over the Greenland sea and the Barents Sea when the subsequent winter Niño-3.4 SST index is positive (Fig. 1a–c). As the structures of the ASIC anomalies are similar in these 3 months, we will focus on the winter mean (D(−1)JF(0), Fig. 1d) in the following analysis. Very similar results are obtained based on the ERSSTv5 and HadISST SST datasets (please see Figs. S1 and S2 in the supporting material). It should be mentioned that the region with obvious ASIC anomalies related to the following winter Niño-3.4 SST anomaly coincides well with the region with large interannual variability of winter ASIC (please see Fig. S3a). In addition, the distribution of ASIC anomalies is similar to the spatial pattern of the first empirical orthogonal function (EOF) mode of D(−1)JF(0) ASIC anomalies (please see Fig. S3b). This implies that the leading interannual variability of the winter ASIC anomalies has a close relation with the following winter ENSO occurrence.

The connection of the winter ASIC change over the Greenland–Barents Seas (GBS) with the subsequent winter ENSO is confirmed by the temporal variation of an ASIC index and the Niño-3.4 index. Figure 2 displays time series of the standardized raw D(−1)JF(0) ASIC index (described in the Sect. 2) and the D(0)JF(1) Niño-3.4 index obtained from three SST datasets as well as their high-pass filtered interannual components. The raw ASIC index shows a clear

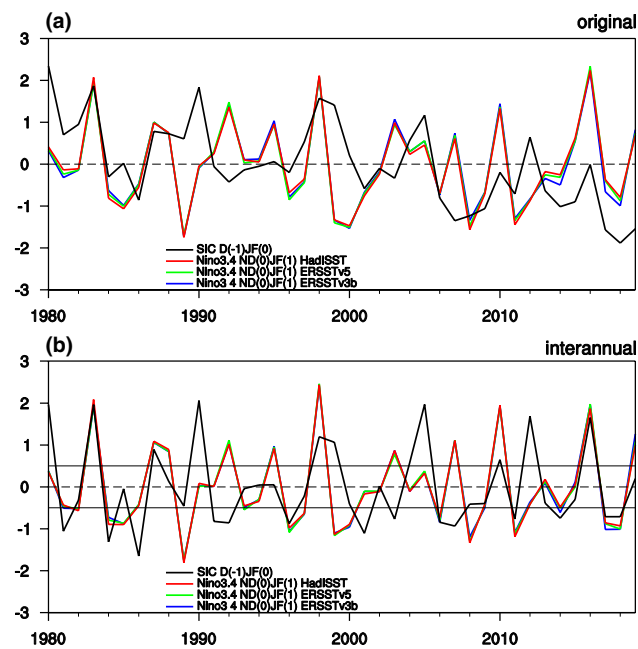


Fig. 2 **a** Time series of original $D(-1)JF(0)$ ASIC index and $D(0)JF(1)$ Niño-3.4 index. **b** Interannual variations of the $D(-1)JF(0)$ ASIC index and $D(0)JF(1)$ Niño-3.4 index. ASIC index is defined as area-mean ASIC anomalies averaged over the region of 70° – 80° N, 10° W– 50° E (i.e. the black box region shown in Fig. 1). Note that the ASIC anomalies have been weighted by the cosine of the latitude to account for decrease of area towards north before calculating the ASIC index

Table 1 Correlation coefficients between the $D(-1)JF(0)$ ASIC index and $D(0)JF(1)$ Niño-3.4 index during 1980–2019

	ERSSTv3b	ERSSTv5	HadISST
Interannual	0.46	0.46	0.46
Original	0.25	0.24	0.26

Three SST datasets (i.e. ERSSTv3b, ERSSTv5, and HadISST) are employed to calculate the Niño-3.4 index. Definitions of the $D(-1)JF(0)$ ASIC index and $D(0)JF(1)$ Niño-3.4 index are provided in the text. The correlation coefficients in the first row are based on interannual components and those in the second row are based on original anomalies

decreasing trend during the analysis period (Fig. 2a), consistent with previous studies (e.g., Comiso et al. 2008; Cavalieri and Parkinson 2012). There is no obvious long-term

linear trend in the original $D(0)JF(1)$ mean Niño-3.4 SST index (Fig. 2a). The correlation coefficients between the original $D(-1)JF(0)$ ASIC index and the $D(0)JF(1)$ Niño-3.4 index obtained from the three SST datasets are low and statistically insignificant during 1980–2019 (Table 1). On the interannual timescale, however, the correlation coefficients between the $D(-1)JF(0)$ ASIC index and the $D(0)JF(1)$ Niño-3.4 SST indices based on ERSSTv3b, ERSSTv5, and HadISST are about 0.46 during 1980–2019, all significant at the 99% confidence level (Table 1). Hence, the winter ASIC has a close relationship with the following winter ENSO on the interannual timescale. In addition, previous studies indicated that ENSO tends to have a 2–7 year period (e.g., Jin et al. 2006; Wang et al. 2008). A power spectrum analysis shows that the winter ASIC index has a significant spectral peak around 2.5 year (please see Fig. S4 in the supporting material).

The connection between ASIC and ENSO is confirmed by examining tropical Pacific SST anomalies following more or less ASIC. We select years with positive and negative $D(-1)JF(0)$ ASIC index according to 0.5 standard deviations. Table 2 lists the selected years with positive and negative winter ASIC index. From Table 2, most of the positive $D(-1)JF(0)$ ASIC index years (1979, 1982, 1986, 1997, 2004, 2009, and 2015) are followed by an El Niño event in the following winter, and many negative $D(-1)JF(0)$ ASIC index years (1983, 1983, 1995, 2000, 2005, 2010, 2016, 2017) are succeeded by a La Niña event in the following winter. In particular, the three strong El Niño events in the past (i.e. 1982–1983, 1997–1998, and 2015–2016) were preceded by strong positive winter ASIC index values. This suggests that the preceding winter ASIC anomaly may be a good indicator of the El Niño occurrence.

The connection between ASIC and ENSO is confirmed by spatial distribution of anomalies in the Pacific region associated with winter ASIC. Figure 3 shows the difference of composite anomalies of SST and precipitation in $D(0)JF(1)$ between positive and negative $D(-1)JF(0)$ ASIC index years. Figure 4 presents the associated anomalies of 200 hPa geopotential height, 850 hPa winds, and SLP in $D(0)JF(1)$. Corresponding to increase in the $D(-1)JF(0)$ ASIC, a notable El Niño-like SST anomaly pattern appears in the tropical Pacific (Wang et al. 2000; McPhaden et al. 2006; Chen et al. 2014a), with SST warming in the TCEP and the subtropical WNP around 20° – 40° N as well as SST cooling

Table 2 List of the positive and negative $D(-1)JF(0)$ ASIC index years

Positive ASIC index years	Negative ASIC index years
1979, 1982, 1986, 1989, 1997, 1998, 2003, 2004, 2009, 2011, 2015	1980, 1983, 1985, 1990, 1991, 1995, 2000, 2002, 2005, 2006, 2010, 2013, 2016, 2017

Positive and negative $D(-1)JF(0)$ ASIC index years are selected according to 0.5 standard deviations

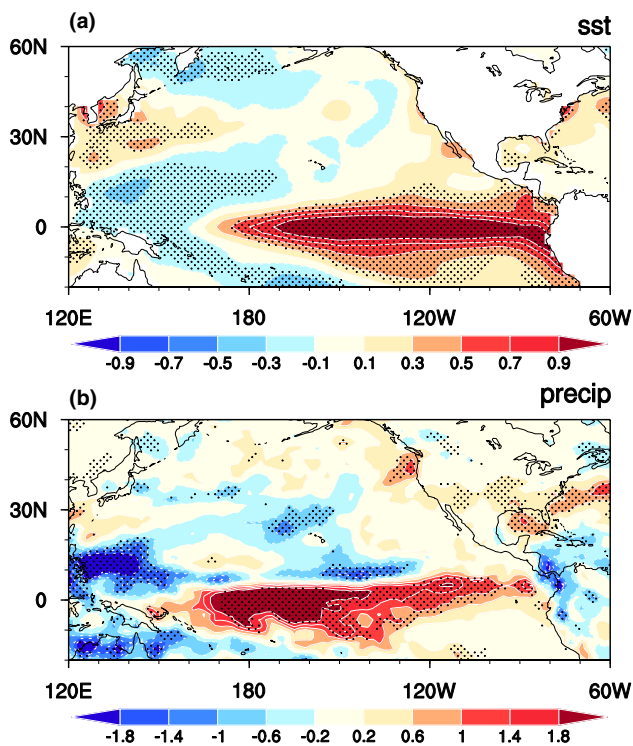


Fig. 3 Difference of composite anomalies of D(0)JF(1) **a** SST (unit: °C) and **b** precipitation (unit: mm day⁻¹) between positive and negative D(-1)JF(0) ASIC index years. Stippling regions in **a**, **b** indicate anomalies that are significantly different from zero at the 95% confidence level

in the tropical WNP around 120°–160°E (Fig. 3a). Significant positive precipitation anomalies, indicating enhanced atmospheric convection activity, are found over the TCEP and negative precipitation anomalies are seen over the western Pacific as a response to the SST anomalies (Fig. 3a, b).

The D(-1)JF(0) mean ASIC-related atmospheric circulation anomalies in following winter (Fig. 4) resemble those related to an El Niño event (Wang et al. 2000; Alexander et al. 2002; McPhaden et al. 2006). At the upper-troposphere, negative geopotential height anomalies are seen over the high latitude North Pacific (Fig. 4a). Notable positive geopotential height anomalies appear in the tropics, which are likely a response to the SST warming in the TCEP (Figs. 3a, 4a) (Wang et al. 2000; Alexander et al. 2002). At 850 hPa, large westerly wind anomalies are seen over the TCEP (Fig. 4b), which are coupled with the SST warming and above-normal precipitation there (Fig. 3) via the Bjerknes-like air–sea feedback mechanism (Bjerknes 1969; Wang et al. 2000; Alexander et al. 2002; Chen et al. 2014a). Meanwhile, the subtropical North Pacific is dominated by an anomalous anticyclone, consistent with positive SLP anomalies there (cf., Fig. 4b with c). Anticyclonic wind anomalies are observed around the South China Sea and the Philippine, with southerly wind anomalies over East Asia and easterly

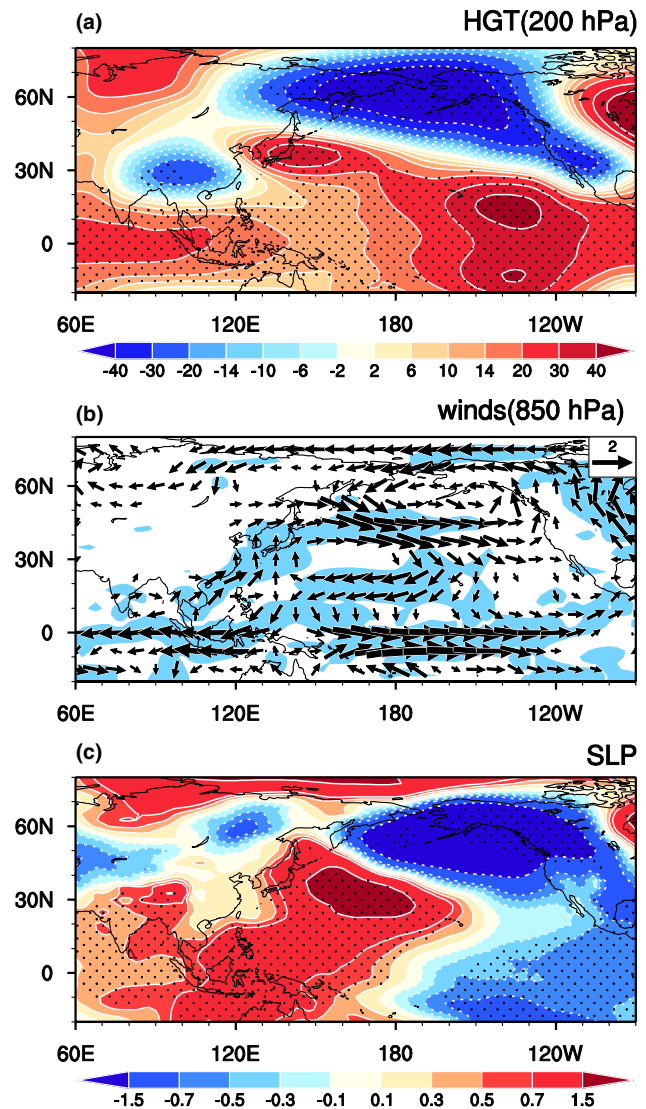


Fig. 4 Composite anomalies of D(0)JF(1) **a** 200 hPa geopotential height (m), **b** 850 hPa winds (m s⁻¹), and **c** SLP (hPa) between positive and negative phases of D(-1)JF(0) ASIC index. Stippling regions in **a** and **c** indicate anomalies that are significantly different from zero at the 95% confidence level. The shading areas in **b** indicate either component of the wind anomalies that are significantly different from zero at the 95% confidence level

wind anomalies around the Maritime Continent and tropical eastern Indian Ocean. Notice that above described atmospheric circulation anomalies also bear a resemblance to the Kuroshio anticyclone suggested by Son et al. (2014) and Kim et al. (2018), which were induced by convection anomalies over the western North Pacific.

Surface temperature displays significant increase over many portions of East Asia (not shown), which is likely related to anomalous southerly winds that bring warmer and wetter air northward from lower latitudes. This indicates that the winter ASIC change partially contributes to

the subsequent winter weather and climate variability over East Asia and the surrounding areas via modulating the following winter ENSO (Zhang et al. 1999; Wang et al. 2000; Chen et al. 2000; Alexander et al. 2002). The spatial distribution of the SLP anomaly over tropical Pacific resembles the Southern Oscillation (Peixoto and Oort 1992; Wang et al. 2000; Alexander et al. 2002; Chen et al. 2014a). The marked negative SLP anomalies over the mid-latitude North Pacific indicate an enhanced Aleutian Low (Overland et al. 1999).

The above analyses demonstrate that the change in winter ASIC over the Greenland–Barents Seas is followed by ENSO features in the subsequent winter in the tropical and mid-latitude North Pacific as well as climate anomalies in the surrounding regions similar to those of ENSO events. These results collectively confirm a close time-lag connection between winter ASIC and the following winter ENSO events.

4 Mechanisms for the influence of the ASIC on ENSO

In this section, we investigate the physical processes linking the winter ASIC change over the GBS to the following winter ENSO. We first document the winter ASIC related atmospheric anomalies during the simultaneous winter. Then, we examine the formation of SST anomalies in the tropical Pacific. After that, we show the coupled evolution of anomalies in the tropical Pacific.

4.1 Atmospheric anomalies in simultaneous $D(-1)JF(0)$

Large atmospheric circulation anomalies span the mid-high latitude Eurasian continent and the North Pacific (Fig. 5). The atmospheric circulation anomalies display a quasi-barotropic vertical structure over Eurasia and the North Pacific (Fig. 5a, b). Pronounced negative geopotential height and cyclonic anomalies occur over the mid-high latitudes of Eurasia, and the subtropical western-central North Pacific around 10° – 30° N (Fig. 5a, b). Meanwhile, a marked anticyclonic anomaly and positive geopotential height anomalies are present over the mid-latitude North Pacific (Fig. 5a, b). In particular, significant westerly wind anomalies are observed over the tropical western-central North Pacific (Fig. 5b). Previous studies have demonstrated that anomalous westerly (easterly) winds over the tropical western-central Pacific play an important role in triggering the El Niño (La Niña) outbreak during the following winter via stimulating eastward propagating warm (cool) Kelvin waves (Yu and Rienecker 1998; Lengaigne et al. 2004; Chen et al. 2014a, 2016a). ENSO events tend to be initiated in early spring (Philander 1985; Barnett et al. 1989; Yu and

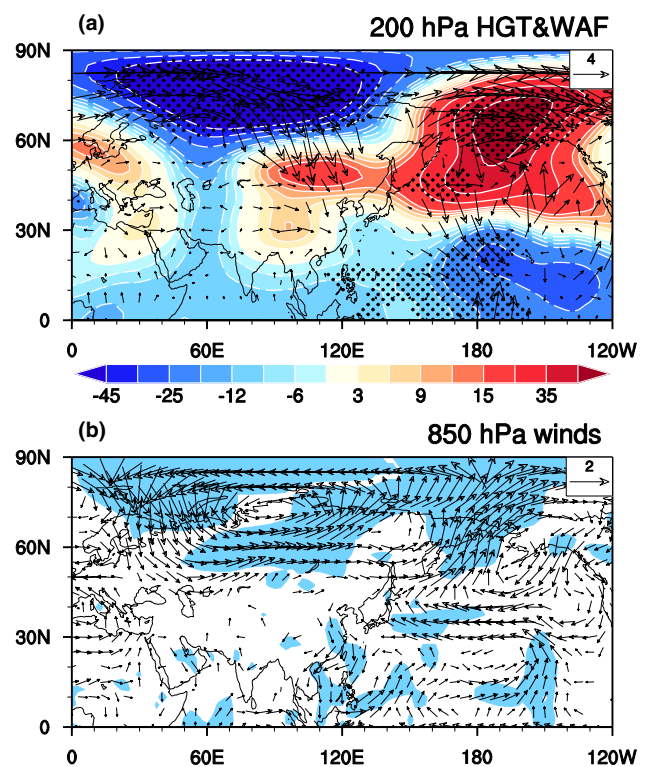


Fig. 5 Difference of composite anomalies of $D(-1)JF(0)$ **a** 200 hPa geopotential height (shadings, m) and wave activity flux (vectors, $\text{m}^2 \text{s}^{-2}$), **b** 850 hPa winds (m s^{-1}) between positive and negative $D(-1)JF(0)$ ASIC index years. Stippling regions in **a** indicate geopotential height anomalies that are significantly different from zero at the 95% confidence level. The shading areas in **b** indicate either component of the wind anomalies that are significantly different from zero at the 95% confidence level

Rienecker 1998; Yu et al. 2003; Chen et al. 2018c). Hence, the ASIC associated westerly wind anomalies over the tropical western-central North Pacific likely play a crucial role in connecting the winter ASIC to the subsequent winter ENSO.

The formation of negative geopotential height and associated cyclonic anomalies over the tropical WNP appears to be related to a southeastward propagating atmospheric teleconnection wave train (Fig. 5a). The propagation of atmospheric wave train from Eurasian Arctic southeastward to the subtropical WNP can be well illustrated by the wave activity fluxes (Fig. 5a). It is noted that the atmospheric circulation anomalies over Eurasia related to the winter ASIC anomalies is largely similar to those identified by Wu et al. (2016). Wu et al. (2016) demonstrated that increases (decreases) in the winter ASIC in the Norwegian Sea and the Barents Sea could trigger an atmospheric wave pattern propagating from Eurasian Arctic to East Asia, with a cyclonic (anticyclonic) anomaly over the high latitudes of Eurasia (please see their Fig. 3), which would be further confirmed by a simple general circulation model experiment. From Fig. 5a, wave activity fluxes are also observed to propagate from the North

Atlantic. This implies that the atmosphere–ocean conditions over the North Atlantic Ocean may also partly contribute to the winter ASIC changes, which remains to be explored.

Previous studies have demonstrated that divergence (convergence) anomalies in the upper troposphere caused by the ascending (descending) motion act as an effective Rossby wave source (RWS) (Sardeshmukh and Hoskins 1988; Watanabe 2004). It is speculated that the ASIC anomalies around the GBS may induce anomalous RWS in the upper troposphere via anomalous ascending or descending motion. To verify this, we calculate the RWS and 500 hPa omega anomalies. Figure 6 displays the difference of composite anomalies of $D(-1)JF(0)$ RWS and 500 hPa omega between positive and negative $D(-1)JF(0)$ ASIC index years. From Fig. 6, strong positive RWS anomalies are observed around the Greenland–Barents Seas, together with significant downward motion anomalies corresponding to increase in the ASIC. In addition, there are pronounced upper-level (200 hPa) convergence anomalies there (not shown). These results indicate that the $D(-1)JF(0)$ ASIC anomalies around the Greenland–Barents Seas are able to

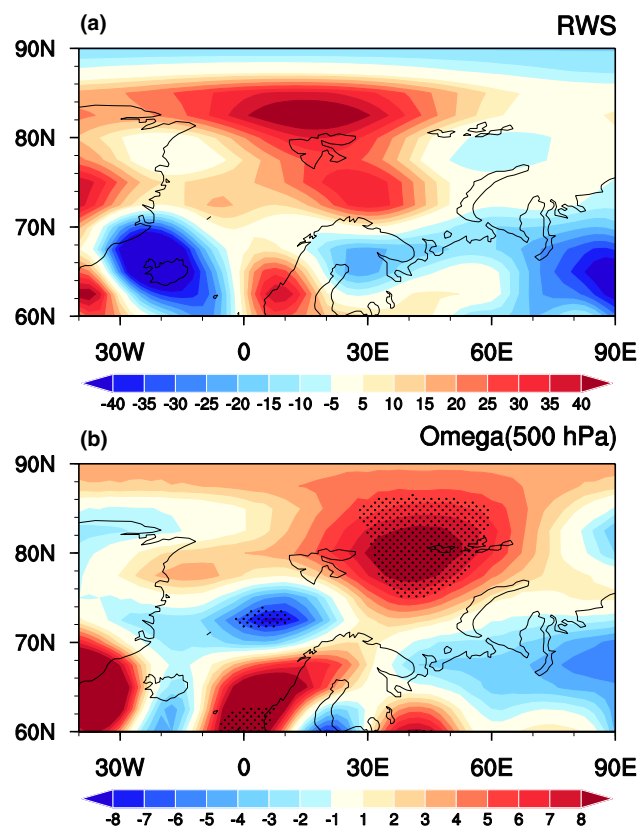


Fig. 6 Difference of composite anomalies of $D(-1)JF(0)$ Rossby wave source (10^{-12} s^{-2} , only values larger than 10×10^{-12} are shown) and 500 hPa omega (hPa s^{-1}) between positive and negative $D(-1)JF(0)$ ASIC index years. Stippling regions in **b** indicate the omega anomalies that are significantly different from zero at the 95% confidence level

trigger a southeastward propagating Rossby wave via the upper-level convergence.

The role of the RWS forcing over the Arctic in the generation of the observed atmospheric wave train is further illustrated by results of model experiments. We perform simulations with a barotropic model (Sardeshmukh and Hoskins, 1988) with anomalous divergence imposed. According to previous studies (Sardeshmukh and Hoskins 1988; Chen et al. 2016b), the barotropic model can well distinguish the key dynamics of atmospheric response to the prescribed convergence or divergence anomaly. The barotropic model used in the present study is spectral with the truncation at rhomboidal wave-number 40. In the following, two experiments with the barotropic model were performed: one with climatological $D(-1)JF(0)$ mean divergence (Exp_Clm) and the other with climatological $D(-1)JF(0)$ divergence plus prescribed convergence anomaly over the Greenland–Barents Seas (Exp_Arc). The convergence anomaly in Exp_Arc has a maximum intensity of $-7 \times 10^{-6} \text{ s}^{-1}$ at 80°N , 30°E . The location of the convergence anomaly is selected according to the region with large values of RWS and significant downward motion anomaly around the Barents Sea in Fig. 6. The barotropic model is integrated for 40 days in the above two experiments.

Figure 7 shows the difference of responses between the Exp_Clm and Exp_Arc averaged over the model days 31–40 with white contours indicating the prescribed convergence anomaly. The spatial pattern of height anomalies over Eurasia and the North Pacific bears a resemblance to that in the observations though the center of negative geopotential height anomalies shifts slightly northward over the North Pacific (cf., Fig. 7 with Fig. 6). This confirms that $D(-1)JF(0)$ ASIC changes over the Greenland–Barents Seas play an important role in forming negative geopotential height anomalies over the subtropical North Pacific via triggering

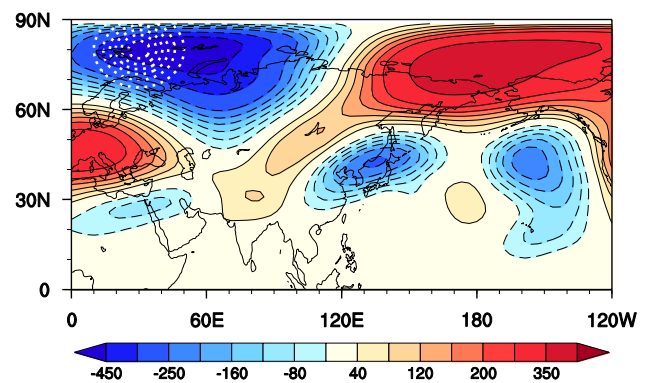


Fig. 7 Barotropic model height perturbation (shading, m) averaged over days 31–40 in response to imposed idealized convergence anomaly (white contours with an interval of 10^{-6} s^{-1} , zero line is omitted) over the Arctic (center of action at 80°N , 30°E)

an atmospheric wave train, generally consistent with Wu et al. (2016).

4.2 Atmospheric heating and SST anomalies at D(–1)JF(0)

Previous studies suggested that the westerly wind anomalies over the WTP are usually accompanied by enhanced atmospheric heating over the tropical WNP (Li 1990; Nakamura et al. 2006, 2007; Chen et al. 2014a). The enhanced atmospheric heating over the tropical WNP induces a significant cyclonic anomaly and associated westerly wind anomalies to its south flank over the WTP via a Gill type atmospheric response (Gill 1980; Li 1990; Nakamura et al. 2007). The anomalous westerly winds induced by the anomalous atmospheric heating further trigger eastward propagating warm Kelvin waves and influence the outbreak of El Niño event in the subsequent winter. Nakamura et al. (2007) also found that the atmospheric heating induced by anomalous northerly winds related to the spring AO over the tropical WNP plays a crucial role in generating the westerly wind anomalies over the WTP via a Gill type atmospheric response. We examine the atmospheric heating anomalies related to the winter ASIC change in the following. Many previous studies have demonstrated that precipitation anomalies can represent atmospheric heating anomalies to a large extent (Yu and Zwiers 2007; Chen et al. 2014a, 2015). Hence, the precipitation anomaly is used here to characterize anomalous atmospheric heating. Significant positive precipitation anomalies are seen over the tropical WNP (Fig. 8). The formation of these positive precipitation anomalies is likely related to northerly wind anomalies around the Philippine Sea and the low-level convergence anomalies associated with the cyclonic anomaly over the WNP (Fig. 5). The enhanced

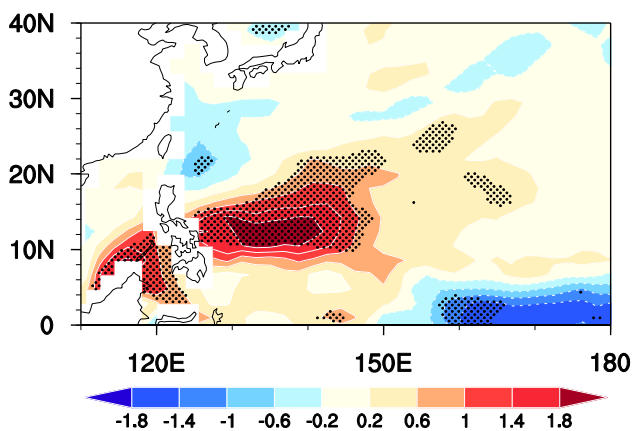


Fig. 8 Difference of composite anomalies of D(–1)JF(0) precipitation (mm day^{-1}) between positive and negative D(–1)JF(0) ASIC index years. Stippling regions indicate anomalies that are significantly different from zero at the 95% confidence level

atmospheric heating anomalies over the WNP contribute to westerly wind anomalies over the tropical WTP through a Gill-type atmospheric response as discussed above.

Does the formation of the atmospheric heating anomalies over the tropical WNP attribute to the underlying SST warming? Figure 9 presents the difference of composite anomalies of SST and 850 hPa winds in D(–1)JF(0), MAM(0), JJA(0), and SON(0) between positive and negative D(–1)JF(0) ASIC index years. The SST anomalies in the North Pacific are weak and insignificant in D(–1)JF(0) (Fig. 9a). This suggests that the formation of the winter atmospheric heating anomalies over the WNP is not attributed to the underlying SST change. In addition, it is noted that SST anomalies in the tropical Pacific are weak and statistically insignificant in D(–1)JF(0). This implies that winter tropical Pacific SST anomalies have a weak relation with the simultaneous winter ASIC change over the Greenland–Barents Seas. In MAM(0), significant SST warming begins to appear in the tropical central Pacific and extends northeastward to the subtropical Pacific (Fig. 9b). These positive spring SST anomalies in the subtropical North Pacific play a role in inducing westerly wind anomalies over the WTP during spring via a Gill-type atmospheric response (Gill 1980; Xie and Philander 1994; Vimont et al. 2003; Chen et al. 2014a). Actually, several previous studies have indicated that the spring SST warming in the subtropical North Pacific is a favorable SST anomaly pattern for the following winter ENSO occurrence via triggering westerly wind anomalies over the tropical western Pacific (Vimont et al. 2001, 2003; Chiang and Vimont 2004; Wang et al. 2012; Chen et al. 2014a). The formation of these SST anomalies in the subtropical North Pacific during spring can be attributed to the preceding winter southerly wind anomalies (Figs. 5a, 9a), which will be further examined later through an analysis of surface heat fluxes. In JJA(0), pronounced SST warming occurs in the TCEP, which is attributed to the westerly wind anomalies over the WTP via triggering eastward propagating warm Kelvin wave (as described below). Subsequently, via the Bjerknes positive air–sea feedback, the SST warming in the TCEP can maintain and develop into following autumn and winter (Bjerknes 1969).

Figure 10 displays the difference of composite anomalies of D(–1)JF(0) surface net heat flux along with its four components (including surface latent and sensible heat fluxes, and surface net shortwave and longwave radiations) between positive and negative D(–1)JF(0) ASIC index years. Values of surface heat fluxes are taken to be positive (negative) when the direction is downward (upward) to warm (cool) SST. Significant and positive surface net heat flux anomalies are found over northern tropical central Pacific. This indicates that the SST warming in the tropical–subtropical central Pacific in the following spring is contributed by surface net heat flux changes. Pronounced positive net heat flux

Fig. 9 Difference of composite anomalies of SST (shadings, °C) and 850 hPa winds (vectors, m s^{-1}) at **a** D(-1) JF(0), **b** MAM(0), **c** JJA(0), **d** SON(0) between positive and negative D(-1)JF(0) ASIC index years. Stippling regions in **a–d** indicate SST anomalies that are significantly different from zero at the 95% confidence level

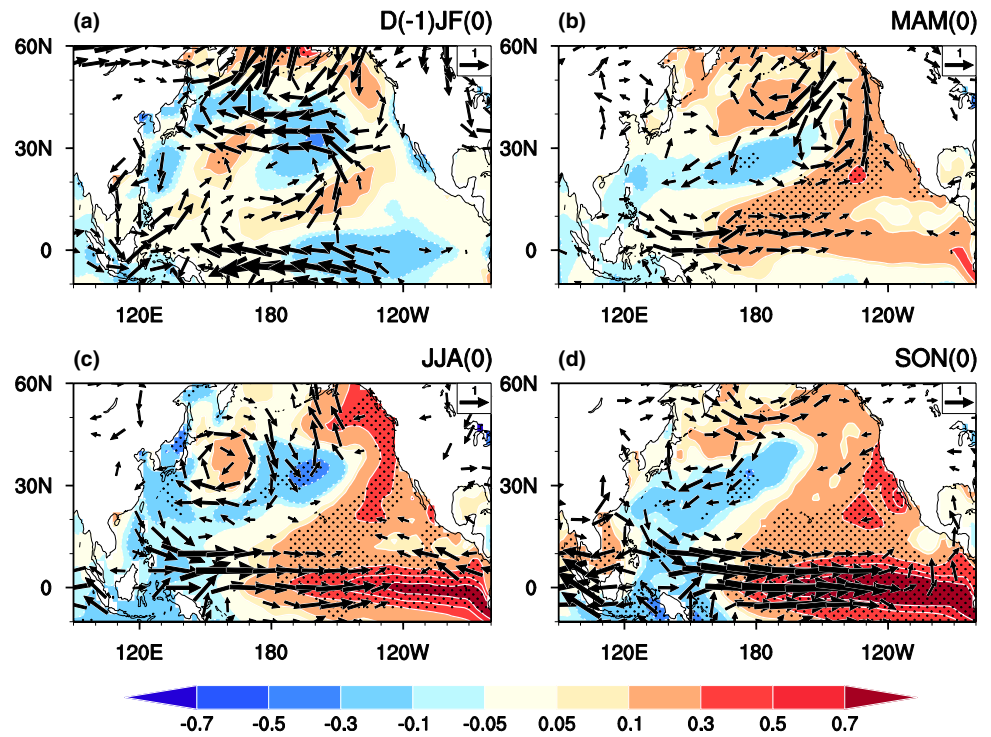
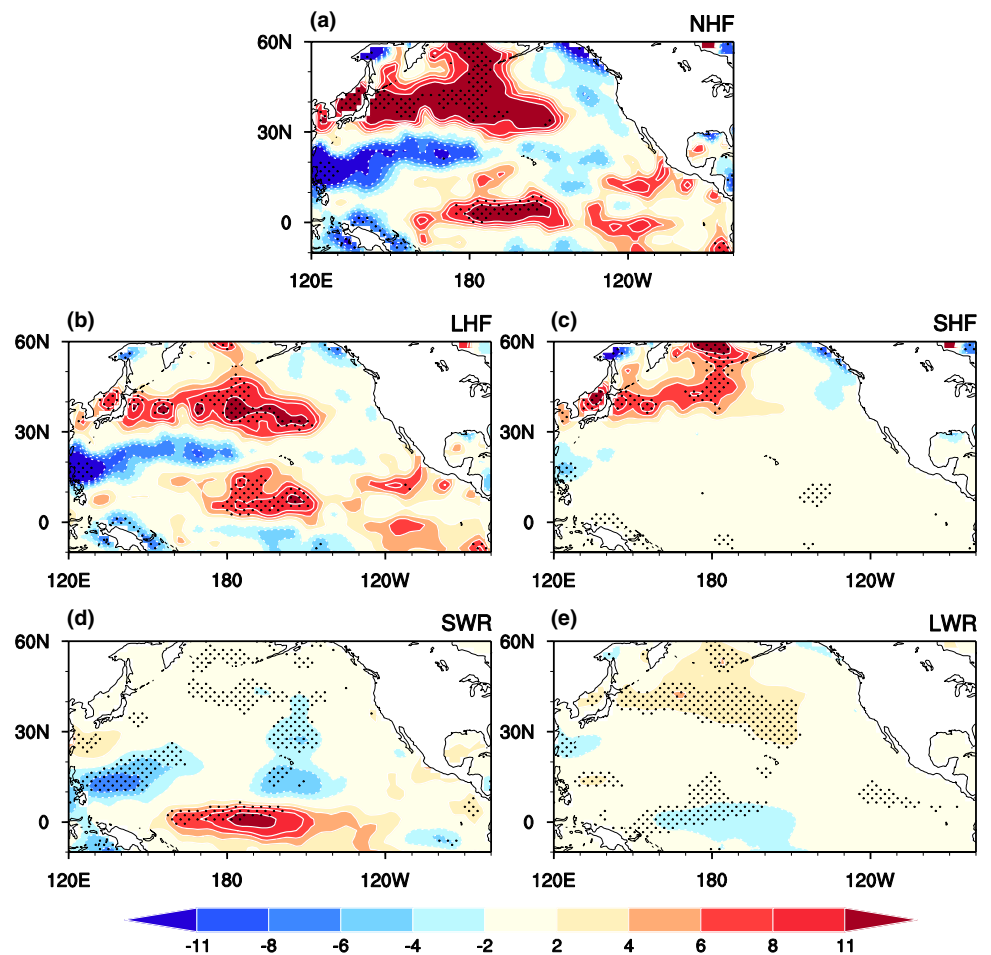


Fig. 10 Difference of composite anomalies (W m^{-2}) of D(-1) JF(0) surface **a** net heat flux, **b** latent heat flux, **c** sensible heat flux, **d** shortwave radiation, and **e** longwave radiation between positive and negative D(-1) JF(0) ASIC index years. Stippling regions indicate anomalies that are significantly different from zero at the 95% confidence level



anomalies are also seen over the mid-latitudes of the North Pacific and marked negative anomalies extend eastward from the Philippines to the central North Pacific (Fig. 10a). The $D(-1)JF(0)$ ASIC related surface net heat flux anomalies over the North Pacific are dominated by changes in surface latent heat flux (Fig. 10b). The southeasterly wind anomalies over the subtropical central North Pacific and easterly wind anomalies over the mid-latitude North Pacific (Fig. 5a) both reduce wind speed there and contribute to increase in surface latent heat flux (Fig. 10b). In addition, decrease in surface latent heat flux (corresponding to upward direction) around the Philippine Sea is related to anomalous northerly winds that enhance evaporation and atmospheric heating (Figs. 5b, 10b). Significant and positive surface sensible heat flux anomalies appear over the mid-latitude North Pacific, which also contributes to increase in surface net heat flux there (Fig. 10c). By contrast, the anomalies of surface sensible heat flux, and shortwave and longwave radiations over the subtropical North Pacific are weaker compared to those of surface latent heat flux (Fig. 10b–e).

4.3 Evolutions of tropical SST, atmospheric heating and atmospheric circulation

The temporal evolution of atmospheric circulation, SST, and atmospheric heating anomalies over the tropical Pacific is similar to that typical of ENSO events. At 850 hPa, pronounced westerly wind anomalies appear over the WTP around 120° – 135° E from DJF(-1) to AMJ(0), and propagate eastward to the TCEP after MJJ(0) (Fig. 11a). The maintenance of westerly wind anomalies from JFM(0) to MJJ(0) may be attributed to significant SST warming in the subtropical North Pacific. Significant easterly wind anomalies at 850 hPa are apparent over the tropical Indian Ocean from ASO(0) to DJF(1) (Fig. 11a). The zonal wind

anomalies at 200 hPa are almost opposite to those at the 850 hPa (Fig. 11), with significant easterly wind anomalies over the TCEP Pacific after JJA(0). Significant SST warming and positive precipitation and upward motion anomalies occur over the tropical central Pacific after AMJ(0) (Fig. 12). Notable negative surface heat flux anomalies appear over the tropical eastern Pacific since MAM(0), which oppose the SST warming. This indicates that the oceanic dynamic process (warm Kelvin wave) likely plays a crucial role in the formation and maintenance of the SST warming in the tropical eastern Pacific.

To confirm the important role of the eastward propagating warm Kelvin wave generated by the anomalous westerly winds in the formation of the SST warming in the TCEP, we display the difference of composite anomalies of Kelvin wave forcing function (K_f) in $D(-1)JF(0)$, MAM(0), JJA(0), and SON(0) between positive and negative phases of $D(-1)JF(0)$ ASIC index in Fig. 13. As demonstrated in previous studies (Battisti 1988; Vimont et al. 2003; Chen et al. 2014a), positive (negative) values of K_f correspond to an eastward propagating and downwelling (upwelling) Kelvin wave. From Fig. 13, significant positive K_f (red dots) anomalies are seen over the WTP in $D(-1)JF(0)$, consistent with the westerly wind anomalies there. These significant positive K_f anomalies propagate eastward in spring, and are evident in the tropical eastern Pacific in the following summer. Therefore, the generation of the SST warming anomalies in the tropical eastern Pacific in the following summer is related to the eastward propagating warm Kelvin wave induced by anomalous westerly winds over the tropical Pacific.

The SST warming in the TCEP can develop and maintain via a Bjerknes positive air–sea feedback mechanism (Bjerknes 1969; Chen et al. 2014a). The ASIC related tropical processes may be summarized as follows: summer SST

Fig. 11 Evolution of difference of composite anomalies (m s^{-1}) of tropical (2.5°N – 10°N -mean) zonal wind at **a** 850 hPa and **b** 200 hPa between positive and negative $D(-1)JF(0)$ ASIC index years. Stippling regions indicate zonal wind anomalies that are significantly different from zero at the 95% confidence level

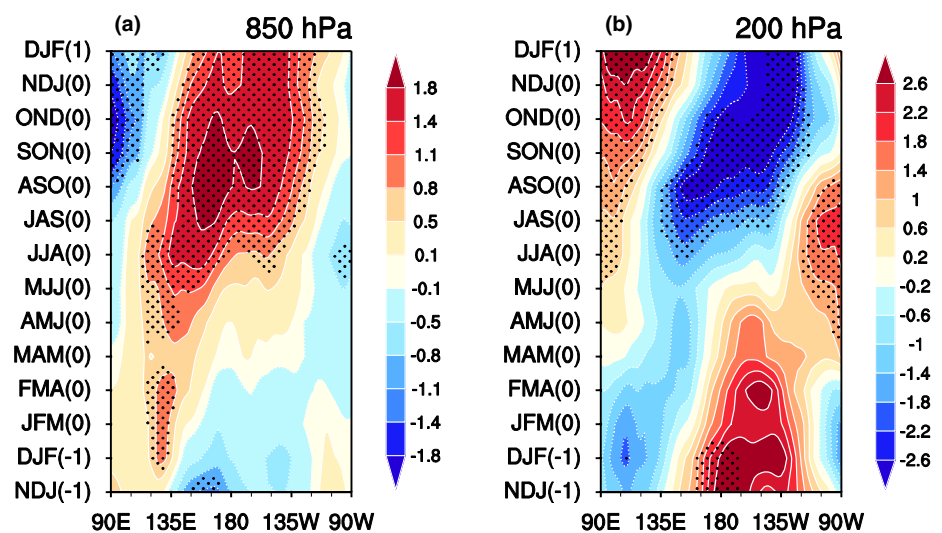


Fig. 12 Evolution of difference of composite anomalies of tropical (5°S–5°N-mean) **a** SST (°C), **b** surface net heat flux (W m^{-2}), **c** precipitation (mm day^{-1}), and **d** 500 hPa omega (hPa s^{-1}) between positive and negative of D(-1)JF(0) ASIC index years. Stippling regions indicate anomalies that are significantly different from zero at the 95% confidence level

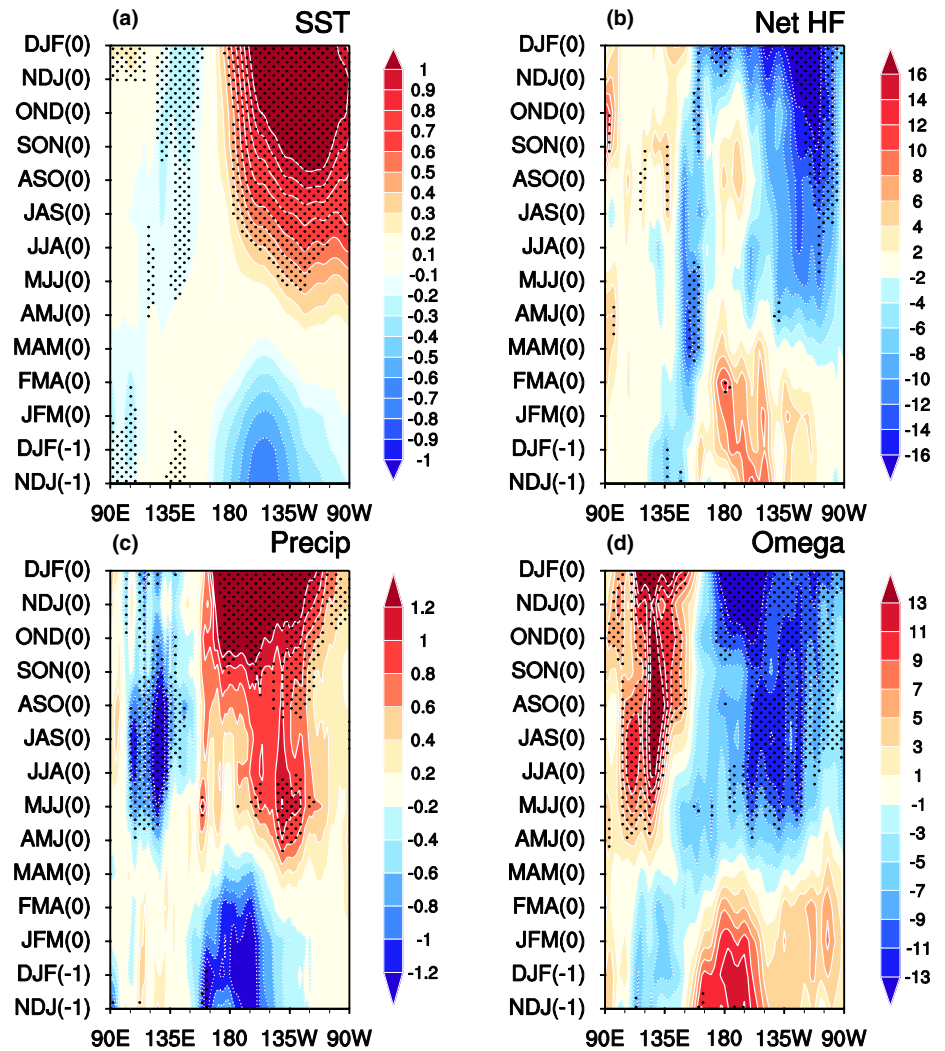
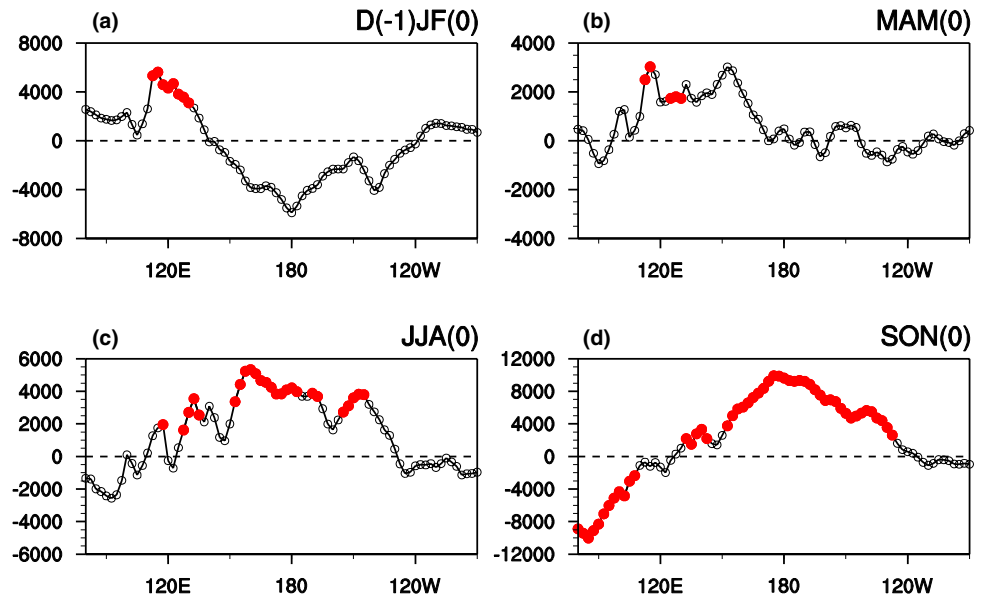


Fig. 13 Difference of composite anomalies of Kelvin wave forcing function at **a** D(-1)JF(0), MAM(0), JJA(0), and SON(0) between positive and negative D(-1)JF(0) ASIC index years. The red dots indicate anomalies that are significantly different from zero at the 95% confidence level



warming in the TCEP induces atmospheric convection and upward motion anomalies (Fig. 12), and maintains anomalous westerly winds at lower level over the TCEP via a Gill-type atmospheric response (Fig. 11). These anomalous westerly winds, in turn, contribute to the enhancement of the TCEP SST warming through eastward propagating warm Kelvin wave (Fig. 13). Through the above processes, an El Niño-like SST warming would be generated in the following winter in the TCEP (Fig. 12a).

In summary, increase in the winter ASIC around the Greenland–Barents Seas induces an anomalous atmospheric wave train propagating from Eurasia to the North Pacific, leading to significant negative geopotential height and cyclonic circulation anomalies over the subtropical North Pacific. The associated atmospheric heating and spring SST warming over the subtropical North Pacific generate and maintain lower-level westerly wind anomalies over the WTP via a Gill-type atmospheric response and the positive wind–evaporation–SST feedback. The induced spring WTP westerly wind anomalies subsequently contribute to summer SST warming in the TCEP via triggering an eastward propagating warm Kelvin wave. Finally, an El Niño event is induced in the following winter via Bjerknes-like positive air–sea feedback.

5 Summary and discussions

Using the NCEP–NCAR reanalysis, ASIC data from the Met Office Hadley Centre, and three SST datasets, this study unravels a close relation between the winter (D(−1)JF(0)) ASIC around the Greenland–Barents Seas and the ENSO in the subsequent winter (D(0)JF(1)). An ASIC index is defined as the area-mean ASIC anomalies over 70°–80°N and 10°W–50°E. The D(−1)JF(0) ASIC index has a significant correlation with the D(0)JF(1) Niño-3.4 index on the interannual timescale, with a correlation coefficient of 0.46 during 1980–2019. An (a) El Niño (La Niña) event tends to occur in the following winter when the ASIC index in preceding winter is in its positive (negative) phase.

The physical processes responsible for the influence of the D(−1)JF(0) ASIC on the following winter ENSO are summarized schematically in Fig. 14. In D(−1)JF(0), an increase in the winter ASIC over the Greenland–Barents Seas induces an atmospheric wave train propagating southeastward from the mid-high latitude Eurasia to the subtropical North Pacific, with negative geopotential height and cyclonic anomalies over Eurasia and the subtropical western-central North Pacific, as well as positive geopotential height anomalies over East Asia and the high-latitude North Pacific. This atmospheric wave train is identified by the wave activity flux and verified by the barotropic model simulations with prescribed convergence

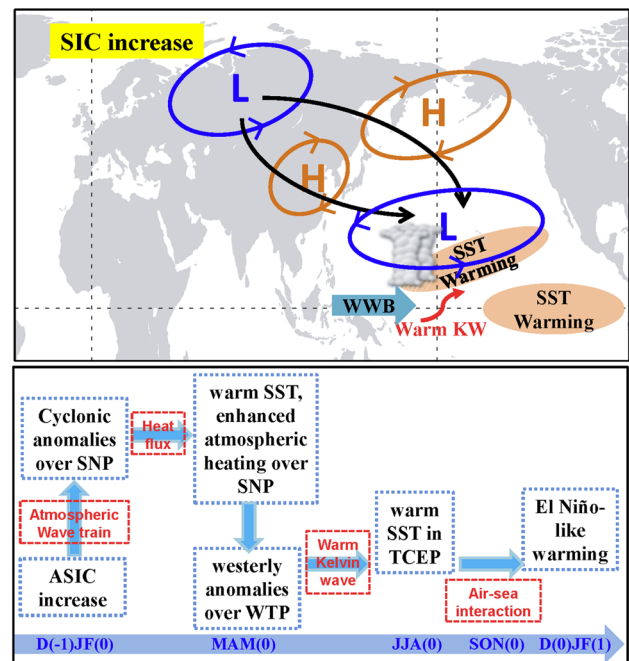


Fig. 14 A schematic diagram displaying the processes linking the winter ASIC changes to the following winter ENSO. Symbol “L” (“H”) indicates negative (positive) geopotential and cyclonic (anticyclonic) anomalies. The black line denotes propagation of atmospheric wave train. Abbreviations of SNP, WTP, and TCEP in the schematic diagram represent subtropical North Pacific, western tropical Pacific, and tropical central-eastern Pacific, respectively

anomalies around the Greenland–Barents Seas. Significant atmospheric heating anomalies are observed over WNP, which is related to the lower-level convergence anomalies over the WNP associated with the cyclonic anomaly induced by the ASIC changes. The atmospheric heating anomalies over the WNP further induce marked westerly wind anomalies over the WTP via a Gill-type atmospheric response. In addition, the anomalous southeasterly winds to the southeastern flank of the cyclonic anomalies over the subtropical central Pacific lead to following spring SST warming over the subtropical North Pacific via reducing wind speed. This spring SST warming helps to maintain anomalous westerly winds over the WTP from winter to the following spring via the positive wind–evaporation–SST feedback mechanism. The westerly wind anomalies over the WTP trigger eastward propagating and downwelling Kelvin waves and contribute to SST warming in the following summer in the TCEP. The SST warming develops and maintains via a positive coupling feedback with the atmospheric circulation and heating, which finally results in the appearance of an El Niño-like SST pattern in the TCEP in the following winter. This study suggests that the change in the winter ASIC is a potential predictor in the occurrence of ENSO in the following winter.

As mentioned in the introduction, SST anomalies in the tropical central-eastern Pacific could induce ASIC anomalies via inducing atmospheric teleconnection (Jevrejeva et al. 2003; Liu et al. 2004; Hu et al. 2016). Meanwhile, ENSO tends to have a strong quasi-biennial variability. An important question is: whether the close relation between the winter ASIC around the Greenland–Barents Seas and the following winter ENSO identified in this study is attributed to the ENSO cycle? To address this question, we have calculated correlation of the $D(-1)JF(0)$ ASIC index with simultaneous winter Niño-3.4 index. It is found that the correlation coefficient between the $D(-1)JF(0)$ ASIC index and the $D(-1)JF(0)$ Niño-3.4 index is fairly weak ($r = -0.18$) during 1980–2019, consistent with the results shown in Fig. 9a. This indicates that winter tropical central-eastern Pacific SST anomalies have a weak relation with the simultaneous winter ASIC anomalies around the Greenland–Barents Seas on the interannual timescale. Furthermore, we remove the $D(-1)JF(0)$ Niño-3.4 index from the $D(-1)JF(0)$ ASIC index, $D(0)JF(1)$ Niño-3.4 index, and other variables via the least squares method. After removing the winter ENSO signal, correlation coefficient between the winter ASIC index and the following winter Niño-3.4 index is still significant at the 99% confidence level ($r = 0.41$). Furthermore, evolutions of the atmospheric circulation and SST anomalies remain almost the same. Hence, the significant winter ASIC-following winter ENSO relation is not due to the ENSO cycle (i.e. quasi-biennial fluctuation of ENSO).

In addition, Wang et al. (2011) has demonstrated that anomalous summer SST over the North Atlantic is also an important factor for the subsequent El Niño evolution via triggering an East Atlantic/West Russia teleconnection-like atmospheric wave train over Eurasia. The atmospheric circulation anomalies over Eurasia induced by the summer North Atlantic SST may both influence winter ASIC around the Greenland–Barents Seas and the following ENSO evolution. Hence, another question is: whether the close connection of the winter ASIC with following winter ENSO was due to previous summer SST anomalies over the North Atlantic. We have examined evolutions of SST anomalies in North Atlantic from previous summer to simultaneous winter (figures not shown). Results found that SST anomalies in North Atlantic during previous summer and autumn related to the winter ASIC index are fairly weak. In particular, following Wang et al. (2011), we have constructed a summer North Atlantic SST index as region-averaged SST anomalies over 30° – 50° N and 10° – 50° W. It is found that the correlation coefficient between $D(-1)JF(0)$ ASIC index and previous summer North Atlantic SST index is insignificant ($r = -0.16$). This result confirms that the winter ASIC-following winter ENSO connection was independent of the Atlantic SST anomalies. It should be mentioned that the winter atmospheric anomalies over North Pacific

induced by the winter ASIC anomalies around the Greenland–Barents Seas bear several resemblances to that related to the North Pacific Oscillation (NPO, Vimont et al. 2001, 2003). This suggests that winter ASIC anomalies may also affect the ENSO evolution via triggering the seasonal footprinting mechanism processes related to the NPO (Vimont et al. 2001, 2003).

Chen et al. (2014a) suggested that spring AO is an important extratropical forcing of the following winter ENSO outbreak. The correlation coefficient between the winter ASIC index and its following spring AO index is 0.32 during 1980–2019, significant at the 95% confidence level. A question is whether the relation of the winter ASIC with following winter ENSO is impacted by the spring AO. To address this issue, we remove the spring AO index from its preceding winter ASIC index and from its following winter Niño-3.4 index by means of linear regression. The correlation coefficient between the winter ASIC index and its following winter Niño-3.4 index is still 0.42 for the period 1980–2019 (significant at the 99% confidence level) after removal of signal of the spring AO index. This suggests that the winter ASIC–ENSO relation is very likely independent of the spring AO–ENSO relation though winter ASIC has a close relation with the following spring AO. Nevertheless, the combined impacts of the winter ASIC and its following spring AO on the following winter ENSO need to be further investigated.

Previous studies indicated that autumn ASIC and Eurasian snow cover anomalies could impact following winter–spring climate anomalies over mid-high latitudes of the Northern Hemisphere via inducing AO-like atmospheric anomalies through stratospheric teleconnection (e.g., Cohen and Entekhabi 1999, 2001; Cohen et al. 2007; Nakamura et al. 2015; Yang et al. 2016; Chen and Wu 2018). A question is whether the stratospheric teleconnection plays a role in connecting the winter ASIC anomalies over the Greenland–Barents Seas to the following ENSO occurrence. To address this issue, following previous studies (Yang et al. 2016; Chen and Wu 2018), we have calculated zonal-mean zonal wind anomalies (averaged between 65° and 90° N) obtained by regression upon the winter ASIC index (please see Figure S5 in the supporting material). From Fig. S5, zonal-mean zonal wind anomalies in the stratosphere from winter to spring are weak and statistically insignificant. This suggests that the stratospheric processes may not play a role in contributing to the generation of the winter ASIC-related atmospheric circulation and SST anomalies from winter to spring. Thus, the significant winter ASIC-following winter ENSO relation may be not related to stratospheric processes.

Acknowledgements We thank two anonymous reviewers for their constructive suggestions and comments, which help to improve the paper. This study is supported by the National Natural Science Foundation of

China Grants (41605050, 41530425, and 41775080), and the Young Elite Scientists Sponsorship Program by the China Association for Science and Technology (2016QNRC001).

References

- Alexander MA, Bladé I, Newman M, Lanzante JR, Lau NC, Scott JD (2002) The atmospheric bridge: the influence of ENSO teleconnections on air–sea interaction over the global oceans. *J Clim* 15(16):2205–2231
- Barbero R, Abatzoglou JT, Brown TJ (2015) Seasonal reversal of the influence of El Niño–Southern Oscillation on very large wildfire occurrence in the interior northwestern United States. *Geophys Res Lett* 42(9):3538–3545
- Barnett T, Dümenil L, Schlese U, Roeckner E, Latif M (1989) The effect of Eurasian snow cover on regional and global climate variations. *J Atmos Sci* 46(5):661–686
- Battisti DS (1988) Dynamics and thermodynamics of a warming event in a coupled tropical atmosphere–ocean model. *J Atmos Sci* 45:2889–2919
- Bell GD, Halpert MS, Kousky VE, Gelman ME, Ropelewski CF, Douglas AV, Schnell RC (1999) Climate assessment for 1998. *Bull Am Meteorol Soc* 80(5):1040
- Bjerknes J (1969) Atmospheric teleconnections from the equatorial Pacific. *Mon Weather Rev* 97:163–172
- Burn DH, Whitfield PH (2015) Changes in floods and flood regimes in Canada. *Can Water Resour J* 41(1–2):139–150
- Cavalieri DJ, Parkinson CL (2012) Arctic sea ice variability and trends, 1979–2010. *Cryosphere* 6:881–889
- Chan JCL (2005) Interannual and interdecadal variations of tropical cyclone activity over the western North Pacific. *Meteorol Atmos Phys* 89:143–152
- Chan JCL, Zhou W (2005) PDO, ENSO and the summer monsoon rainfall over South China. *Geophys Res Lett* 32:L08810
- Chen S, Song L (2019) The leading interannual variability modes of winter surface air temperature over Southeast Asia. *Clim Dyn* 52:4715–4734
- Chen S, Wu R (2018) Impacts of early autumn arctic sea ice concentration on subsequent spring Eurasian surface air temperature variations. *Clim Dyn* 51:2523–2542
- Chen W, Graf HF, Huang RH (2000) The interannual variability of East Asian winter monsoon and its relation to the summer monsoon. *Adv Atmos Sci* 17:48–60
- Chen S, Yu B, Chen W (2014a) An analysis on the physical process of the influence of AO on ENSO. *Clim Dyn* 42(3–4):973–989
- Chen Z, Wu R, Chen W (2014b) Impacts of autumn Arctic sea ice concentration changes on the East Asian winter monsoon variability. *J Clim* 27:5433–5450
- Chen S, Wu R, Chen W, Yu B (2015) Influence of the November Arctic Oscillation on the subsequent tropical Pacific sea surface temperature. *Int J Climatol* 35:4307–4317
- Chen S, Wu R, Chen W, Yu B, Cao X (2016a) Genesis of westerly wind bursts over the equatorial western Pacific during the onset of the strong 2015–2016 El Niño. *Atmos Sci Lett* 17:384–391
- Chen S, Wu R, Liu Y (2016b) Dominant modes of interannual variability in Eurasian surface air temperature during boreal spring. *J Clim* 29:1109–1125
- Chen S, Wu R, Chen W (2018a) A strengthened impact of November Arctic oscillation on subsequent tropical Pacific sea surface temperature variation since the late-1970s. *Clim Dyn* 51:511–529
- Chen S, Chen W, Yu B (2018b) Modulation of the relationship between spring AO and the subsequent winter ENSO by the preceding November AO. *Sci Rep* 8:6943
- Chen S, Yu B, Chen W, Wu R (2018c) A review of atmosphere–ocean forcings outside the tropical Pacific on the El Niño–Southern oscillation occurrence. *Atmosphere* 9:439
- Chen S, Wu R, Chen W (2019a) Enhanced impact of Arctic sea ice change during boreal autumn on the following spring Arctic oscillation since the mid-1990s. *Clim Dyn*. <https://doi.org/10.1007/s00382-019-04886-y>
- Chen S, Wu R, Song L, Chen W (2019b) Interannual variability of surface air temperature over mid-high latitudes of Eurasia during boreal autumn. *Clim Dyn* 53:1805–1821. <https://doi.org/10.1007/s00382-019-04738-9>
- Chiang JCH, Vimont DJ (2004) Analogous Pacific and Atlantic meridional modes of tropical atmosphere–ocean variability. *J Clim* 17(21):4143–4158
- Cohen J, Entekhabi D (1999) Eurasian snow cover variability and Northern Hemisphere climate predictability. *Geophys Res Lett* 26(3):345–348
- Cohen J, Entekhabi D (2001) The influence of snow cover on Northern Hemisphere climate variability. *Atmos Ocean* 39:35–53
- Cohen J, Barlow MA, Kushner PJ, Saito K (2007) Stratosphere–troposphere coupling and links with Eurasian land surface variability. *J Clim* 20(21):5335–5343
- Cohen JL, Furtado JC, Barlow MA, Alexeev VA, Cherry JE (2012) Arctic warming, increasing snow cover and widespread boreal winter cooling. *Environ Res Lett* 7(1):014007
- Comiso JC, Parkinson CL, Gersten R, Stock L (2008) Accelerated decline in the Arctic sea ice cover. *Geophys Res Lett* 35:L01703
- Ding S, Chen W, Graf HF, Guo Y, Nath D (2018) Distinct winter patterns of tropical Pacific convection anomaly and the associated extratropical wave trains in the Northern Hemisphere. *Clim Dyn* 51:2003–2022
- Duchon CE (1979) Lanczos filtering in one and two dimensions. *J Appl Meteorol* 18:1016–1022
- Francis JA, Chan W, Leathers DJ, Miller JR, Veron DE (2009) Winter Northern Hemisphere weather patterns remember summer Arctic sea-ice extent. *Geophys Res Lett* 36:L07503
- Gao Y, Sun J, Li F, He S, Stein S, Yan Q, Zhang Z, Katja L, Noel K, Tore F, Suo L (2015) Arctic sea ice and Eurasian climate: a review. *Adv Atmos Sci* 32:92–114
- Gill AE (1980) Some simple solutions for heat-induced tropical circulation. *Q J R Meteorol Soc* 106:447–462
- Glynn PW, de Weerd WH (1991) Elimination of two reef-building hydrocorals following the 1982–83 El Niño warming event. *Science* 253(5015):69–71
- Graf HF, Zanchettin D (2012) Central Pacific El Niño, the “subtropical bridge” and Eurasian climate. *J Geophys Res* 117:D01102
- Gray WM (1984) Atlantic seasonal hurricane frequency. Part I: El Niño and 30 mb quasi-biennial oscillation influences. *Mon Weather Rev* 112:1649–1668
- Ham YG, Kug JS, Park JY, Jin FF (2013) Sea surface temperature in the north tropical Atlantic as a trigger for El Niño/Southern Oscillation events. *Nat Geosci* 6:112–116
- He S (2015) Asymmetry in the Arctic Oscillation teleconnection with January Cold extremes in Northeast China. *Atmos Ocean Sci Lett* 8:386–391
- He S, Gao Y, Furevik T, Wang H, Li F (2018) Teleconnection between sea ice in the Barents Sea in June and the Silk Road, Pacific–Japan and East Asian rainfall patterns in August. *Adv Atmos Sci* 35:52–64
- Honda M, Inoue J, Yamane S (2009) Influence of low Arctic sea-ice minima on anomalously cold Eurasian winters. *Geophys Res Lett* 36:L08707
- Hu C, Yang S, Wu Q, Li Z, Chen J, Deng K, Zhang T, Zhang C (2016) Shifting El Niño inhibits summer Arctic warming and Arctic sea ice melting over the Canada Basin. *Nat Commun* 7:11721

- Hu C, Zhang C, Song Yang, Chen D, He S (2018) Perspective on the northwestward shift of autumn tropical cyclogenesis locations over the western North Pacific from shifting ENSO. *Clim Dyn* 51:2455–2465
- Huang B et al (2017) Extended Reconstructed Sea Surface Temperature version 5 (ERSSTv5), Upgrades, validations, and intercomparisons. *J Clim* 30:8179–8205
- Jevrejeva S, Moore JC, Grinsted A (2003) Influence of the Arctic Oscillation and El Niño–Southern Oscillation (ENSO) on ice conditions in the Baltic Sea: the wavelet approach. *J Geophys Res* 108:D21
- Jin FF (1997) An equatorial ocean recharge paradigm for ENSO. Part I: Conceptual model. *J Atmos Sci* 54:811–829
- Jin FF, Kim ST, Bejarano L (2006) A coupled-stability index for ENSO. *Geophys Res Lett* 33:L23708
- Kalnay E, Kanamitsu M, Kistler R, Collins W, Deaven D, Gandin L, Iredell M, Saha S, White G, Woollen J (1996) The NCEP/NCAR 40-year reanalysis project. *Bull Am Meteorol Soc* 77:437–471
- Kim SY, Son HY, Kug JS (2018) Relative roles of equatorial central Pacific and western North Pacific precipitation anomalies in ENSO teleconnection over the North Pacific. *Clim Dyn* 51:4345–4355
- Kug JS, Jeong JH, Jang YS, Kim BM, Folland CK, Min SK, Son SW (2015) Two distinct influences of Arctic warming on cold winters over North America and East Asia. *Nat Geosci* 8:759–762. <https://doi.org/10.1038/ngeo2517>
- Latif M et al (1998) A review of the predictability and prediction of ENSO. *J Geophys Res* 14:375–393
- Lau NC, Nath MJ (1996) The role of the ‘‘atmospheric bridge’’ in linking tropical Pacific ENSO events to extratropical SST anomalies. *J Clim* 9:2036–2057
- Lengaigne M, Guilyardi E, Boulanger J-P, Menkes C, Delecluse P, Inness P, Cole J, Slingo J (2004) Triggering of El Niño by westerly wind events in a coupled general circulation model. *Clim Dyn* 23:601–620
- Lewis SL, Brando PM, Phillips OL, van der Heijden GMF, Nepstad D (2011) The 2010 Amazon drought. *Science* 331(6017):554
- Li CY (1990) Interaction between anomalous winter monsoon in East Asia and El Niño Events. *Adv Atmos Sci* 7:36
- Li F, Wang HJ (2013) Relationship between Bering Sea ice cover and East Asian winter monsoon year-to-year variations. *Adv Atmos Sci* 30:48–56
- Li JP, Wu ZW (2012) Importance of autumn Arctic sea ice to northern winter snowfall. *Proc Natl Acad Sci USA* 109:E1898
- Li X, Wu ZW, Li Y (2019) A link of China warming hiatus with the winter sea ice loss in Barents-Kara Seas. *Clim Dyn* 53:2625–2642. <https://doi.org/10.1007/s00382-019-04645-z>
- Liu J, Curry JA, Martinson DG (2004) Interpretation of recent Antarctic sea ice variability. *Geophys Res Lett* 31:L02205
- Liu JP, Curry JA, Wang HJ, Song MR, Horton RM (2012) Impact of declining Arctic sea ice on winter snowfall. *Proc Natl Acad Sci USA* 109:4074–4079
- McPhaden MJ, Zebiak SE, Glantz MH (2006) ENSO as an integrating concept in Earth science. *Science* 314(5806):1740–1745
- Nakamura T, Tachibana Y, Honda M, Yamane S (2006) Influence of the Northern Hemisphere annular mode on ENSO by modulating westerly wind bursts. *Geophys Res Lett* 33:L07709
- Nakamura T, Tachibana Y, Shimoda H (2007) Importance of cold and dry surges in substantiating the NAM and ENSO relationship. *Geophys Res Lett* 34:L22703
- Nakamura T, Yamazaki K, Iwamoto K, Honda M, Miyoshi Y, Ogawa Y, Ukita J (2015) A negative phase shift of the winter AO/NAO due to the recent Arctic sea-ice reduction in late autumn. *J Geophys Res* 120:3209–3227
- Overland JE, Adams JM, Bond NA (1999) Decadal variability of the Aleutian Low and its relation to high-latitude circulation. *J Clim* 12:1542–1548
- Park JY, Yeh SW, Kug JS, Yoon J (2013) Favorable connections between seasonal footprinting mechanism and El Niño. *Clim Dyn* 40:1169–1181
- Peixoto JP, Oort AH (1992) *Physics of climate*. Springer, New York
- Philander SG (1985) El Niño and La Niña. *J Atmos Sci* 42:2652–2662
- Rayner NA, Parker DE, Horton EB, Folland CK, Alexander LV, Rowell DP, Kent EC, Kaplan A (2003) Global analyses of sea surface temperature, sea ice, and night marine air temperature since the late nineteenth century. *J Geophys Res* 108:4407
- Rogers JC (1981) The North Pacific oscillation. *J Climatol* 1(1):39–57
- Ropelewski CF, Halpert MS (1987) Global and regional scale precipitation patterns associated with the El Niño/Southern Oscillation. *Mon Wea Rev* 115(8):1606–1626
- Sardeshmukh PD, Hoskins BJ (1988) The generation of global rotational flow by steady idealized tropical divergence. *J Atmos Sci* 45:1228–1251
- Schopf MJ, Suarez PS (1988) A delayed action oscillator for ENSO. *J Atmos Sci* 45:3283–3287
- Screen JA, Deser C, Simmonds I, Tomas R (2014) Atmospheric impacts of Arctic sea-ice loss, 1979–2009: Separating forced change from atmospheric internal variability. *Clim Dyn* 43:333–344
- Smith TM, Reynolds RW, Peterson TC, Lawrimore J (2008) Improvements to NOAA’s historical merged land-ocean surface temperature analysis (1880–2006). *J Clim* 21:2283–2296
- Son HY, Park JY, Kug JS, Yoo J, Kim CH (2014) Winter Precipitation variation over Korean Peninsula associated with ENSO. *Clim Dyn* 42:3171–3186
- Song LY, Chen S, Chen W, Chen X (2017) Distinct impacts of two types of La Niña events on Australian Summer rainfall. *Int J Climatol* 37:2532–2544
- Takaya K, Nakamura H (1997) A formulation of a wave activity flux for stationary Rossby waves on a zonally varying basic flow. *Geophys Res Lett* 24:2985–2988
- Takaya K, Nakamura H (2001) A formulation of a phase-independent wave activity flux for stationary and migratory quasigeostrophic eddies on a zonally varying basic flow. *J Atmos Sci* 58:608–627
- Thompson DW, Wallace JM (1998) The Arctic Oscillation signature in the wintertime geopotential height and temperature fields. *Geophys Res Lett* 25(9):1297–1300
- Vimont DJ, Battisti DS, Hirst AC (2001) Footprinting: a seasonal connection between the tropics and mid-latitudes. *Geophys Res Lett* 28:3923–3926
- Vimont DJ, Wallace JM, Battisti DS (2003) The seasonal footprinting mechanism in the Pacific: implications for ENSO. *J Clim* 16:2668–2675
- Walker GT, Bliss E (1932) *World weather*. V Mem R Meteorol Soc 4:53–84
- Wang B, Wu R, Fu X (2000) Pacific-East Asian teleconnection: how does ENSO affect East Asian climate? *J Clim* 13(9):1517–1536
- Wang B, Yang J, Zhou T, Wang B (2008) Interdecadal changes in the major modes of Asian-Australian monsoon variability: strengthening relationship with ENSO since the late 1970s. *J Clim* 21:1771–1789
- Wang X, Wang CZ, Zhou W, Wang DX, Song J (2011) Teleconnected influence of North Atlantic sea surface temperature on the El Niño onset. *Clim Dyn* 37(3–4):663–676
- Wang SY, L’Heureux M, Chia HH (2012) ENSO prediction one year in advance using western North Pacific sea surface temperatures. *Geophys Res Lett* 39:L05702
- Watanabe M (2004) Asian jet waveguide and a downstream extension of the North Atlantic Oscillation. *J Clim* 17(24):4674–4691
- Wu R, Hu ZZ, Kirtman BP (2003) Evolution of ENSO-related rainfall anomalies in East Asia. *J Clim* 16:3742–3758

- Wu BY, Su JZ, Zhang RH (2011) Effects of autumn-winter Arctic sea ice on winter Siberian High. *Chin Sci Bull* 56:3220–3228
- Wu ZW, Li XX, Li YJ, Li Y (2016) Potential influence of Arctic sea ice to the interannual variations of East Asian spring precipitation. *J Clim* 29:2797–2813
- Xie SP, Philander SGH (1994) A coupled ocean-atmosphere model of relevance to the ITCZ in the eastern Pacific. *Tellus Ser A Dyn Meteorol Oceanol* 46:340–350
- Xu X, He S, Li F, Wang H (2018) Impact of northern Eurasian snow cover in autumn on the warm Arctic–cold Eurasia pattern during the following January and its linkage to stationary planetary waves. *Clim Dyn* 50:1993–2006
- Yang X, Yuan X, Ting M (2016) Dynamical link between the Barents-Kara sea ice and the Arctic Oscillation. *J Clim* 29:5103–5122
- Yu L, Rienecker MM (1998) Evidence of an extratropical atmospheric influence during the onset of the 1997–98 El Niño. *Geophys Res Lett* 25:3537–3540
- Yu B, Zwiers F (2007) The impact of combined ENSO and PDO on the PNA climate: a 1,000-year climate modeling study. *Clim Dyn* 29:837–851
- Yu L, Weller RA, Liu WT (2003) Case analysis of a role of ENSO in regulating the generation of westerly wind bursts in the western equatorial Pacific. *J Geophys Res* 108(C4):3128
- Zhang Y, Wallace JM, Battisti DS (1997) ENSO-like interdecadal variability: 1900–93. *J Clim* 10(5):1004–1020
- Zhang R, Sumi A, Kimoto M (1999) A diagnostic study of the impact of El Niño on the precipitation in China. *Adv Atmos Sci* 16:229–241

Publisher's Note Springer Nature remains neutral with regard to jurisdictional claims in published maps and institutional affiliations.